

Magnetism of iron and nickel from rotationally invariant Hirsch-Fye quantum Monte Carlo calculations

A. S. Belozerov,^{1,2} I. Leonov,³ and V. I. Anisimov^{1,2}

¹*Institute of Metal Physics, Russian Academy of Sciences, 620990 Yekaterinburg, Russia*

²*Ural Federal University, 620990 Yekaterinburg, Russia*

³*Theoretical Physics III, Center for Electronic Correlations and Magnetism, Institute of Physics, University of Augsburg, 86135 Augsburg, Germany*

(Dated: November 1, 2018)

We present a rotationally invariant Hirsch-Fye quantum Monte Carlo algorithm in which the spin rotational invariance of Hund's exchange is approximated by averaging over all possible directions of the spin quantization axis. We employ this technique to perform benchmark calculations for the two- and three-band Hubbard models on the infinite-dimensional Bethe lattice. Our results agree quantitatively well with those obtained using the continuous-time quantum Monte Carlo method with rotationally invariant Coulomb interaction. The proposed approach is employed to compute the electronic and magnetic properties of paramagnetic α iron and nickel. The obtained Curie temperatures agree well with experiment. Our results indicate that the magnetic transition temperature is significantly overestimated by using the density-density type of Coulomb interaction.

PACS numbers: 71.15.Mb, 71.20.Be, 71.27.+a

I. INTRODUCTION

The theoretical description of the electronic properties of transition metal compounds with partially filled d and f -shells and strong Coulomb interaction between the electrons remains a challenging, fundamental problem in condensed matter physics.^{1,2} The interplay between electronic and lattice degrees of freedom in such materials results in their diverse physical properties and rich phase diagrams making these compounds particularly attractive for technological applications.³ Moreover, orbital degeneracy is an important and often inevitable cause of this complexity. Together with the Hund's exchange interaction, it has important implications for the electronic and magnetic properties of correlated materials, leading to formation of local moments and complicated multiplet structures.

The electronic properties of correlated materials can be understood by employing the so-called LDA+DMFT approach,^{1,4} a combination of *ab initio* local density approximation (LDA) of the density functional theory and dynamical mean-field theory (DMFT). Nowadays, the LDA+DMFT technique has become a state-of-the-art method for realistic description of correlated electron materials from first principles. This approach provides a systematic many-body treatment of the effect of local electronic correlations by taking into account temporal fluctuations while spatial fluctuations are neglected. Applications of LDA+DMFT for correlated electron compounds such as transition metals and their oxides have provided important insights into our understanding of the electronic and magnetic properties of these materials. In particular, by employing the LDA+DMFT technique it has become possible to obtain a good quantitative description of localized as well as delocalized electron states. In addition, the approach allows one to determine the electronic and magnetic properties of correlated com-

pounds in both paramagnetic and magnetically ordered states.

Nevertheless, there are two important limitations of conventional implementations of the LDA+DMFT method. The first originates from the single-site (local) nature of DMFT. In particular, the key assumption of the theory is the limit of infinite spatial dimension, which allows one to perform an exact mapping of a complex lattice model (such as the Hubbard model) to a quantum impurity with an energy-dependent external bath, resulting in k -independent self-energy. However, in some cases the non-local spatial correlations can be essential to provide a correct description of the properties of correlated materials.⁵ For instance, the standard LDA+DMFT calculations are not able to capture the reduction of magnetic transition temperature due to long-wavelength spin waves. To resolve this problem several methods have been recently proposed,⁶ which we leave beyond the scope of our paper.

The second limitation concerns the spin rotational symmetry of the Hund's exchange interaction. Since correlated materials often have several bands at the Fermi level, it requires specific treatment of the local Coulomb interaction, which in a cubic environment consists of the intra- and inter-orbital Coulomb interactions U and U' , Hund's exchange J , and the pair-hopping coupling J' . These interactions obey spin and orbital rotational symmetry, thereby $U = U' + J + J'$ ensures the rotational invariance in the orbital space and $J = J'$ can be assumed whenever the spin-orbital coupling is negligible. Unfortunately, it is difficult to handle all these multi-band interactions including Hund's exchange coupling and the pair hopping term with the quantum Monte Carlo (QMC) method. In particular, a straightforward implementation leads to a severe sign problem making such simulations unfeasible. Therefore, at present, the most material-specific calculations employ the approxi-

mate form of the Coulomb repulsion restricted to the Ising-type exchange interaction. These calculations often provide a good quantitative description of the electronic, magnetic, and structural properties of correlated materials as a function of the reduced temperature T/T_C , where T_C is the calculated temperature of magnetic ordering.^{7,8} However, the correct symmetry of the exchange interaction turns out to be essential for quantitative description of the electronic and magnetic properties of correlated systems.^{9–14}

This problem can be overcome by using some quantum impurity solvers such as numerical renormalization group (NRG),¹⁵ exact diagonalization (ED),¹⁶ continuous-time quantum Monte Carlo (CT-QMC),¹⁷ and others,^{11,13,18} which allow one to treat the Coulomb interaction in its general form with preserved spin rotational symmetry. These calculations performed for the two- and three-band Hubbard models on the infinite-dimensional Bethe^{10,12} and hypercubic¹¹ lattices show a substantial overestimation of the magnetic transition temperature for the approximate Ising-type form of the exchange Coulomb interaction with respect to the rotationally invariant one. In accordance with this, recent LDA+DMFT calculations of correlated compounds also indicate that the magnetic transition temperatures appear to be significantly overestimated by using the density-density type of Coulomb interaction.^{7,13,19} However, applications of these techniques so far have been mostly limited to simple model systems and only a few realistic calculations for 3d compounds have been recently presented.²⁰ This is mostly because of high computational costs (exponential with the number of orbitals) of these methods implemented with the full rotationally invariant Coulomb interaction which makes such calculations for 3d and 4f materials extremely expensive. Obviously, the LDA+DMFT investigations of correlated materials with the Coulomb interaction in its general form with preserved spin rotational symmetry remain problematic and pose a great theoretical challenge.

In this paper, we present an implementation of the LDA+DMFT approach which allows us to take into account rotational symmetry of the exchange Coulomb interaction. This approach is formulated in terms of the Hirsch-Fye quantum Monte Carlo algorithm²¹ where the spin rotational invariance of Hund's exchange is approximated by averaging over all possible directions of the spin quantization axis. It provides a robust and computationally efficient method which allows us to simulate the five-orbital systems at high temperatures. Using this technique we perform benchmark calculations for the two- and three-band Hubbard models on the infinite-dimensional Bethe lattice. In addition, we employ the proposed approach to calculate the electronic and magnetic properties of paramagnetic α iron and nickel. To outline the importance of rotational symmetry of the exchange Coulomb interaction we compare our results with those obtained by using the density-density approximation.

This paper is organized as follows. In Sec. II we present

a detailed formulation of the proposed approach which allows one to treat rotational invariance of the exchange interaction. In Sec. III we employ this technique to compute the electronic and magnetic properties of the two- and three-band models on the Bethe lattice, paramagnetic α iron, and nickel. The obtained results are compared with those of previous calculations and experimental data. Finally, conclusions are presented in Sec. IV.

II. METHOD

The multiband Hamiltonian with full rotationally invariant on-site Coulomb interaction can be written in the following form:²²

$$\begin{aligned} \hat{H} = & U \sum_m \hat{n}_{m\uparrow} \hat{n}_{m\downarrow} \\ & + \frac{1}{2} \sum_{\substack{mm'\sigma \\ m \neq m'}} \{ (U - 2J) \hat{n}_{m\sigma} \hat{n}_{m'\bar{\sigma}} + (U - 3J) \hat{n}_{m\sigma} \hat{n}_{m'\sigma} \\ & - J (\hat{c}_{m\sigma}^\dagger \hat{c}_{m\bar{\sigma}} \hat{c}_{m'\bar{\sigma}}^\dagger \hat{c}_{m'\sigma} + \hat{c}_{m\sigma}^\dagger \hat{c}_{m\bar{\sigma}} \hat{c}_{m'\sigma} \hat{c}_{m'\bar{\sigma}}) \}, \end{aligned} \quad (1)$$

where $\hat{c}_{m\sigma}^\dagger$ ($\hat{c}_{m\sigma}$) denotes the creation (annihilation) operator of an electron with spin σ ($=\uparrow, \downarrow$) at orbital m , $\hat{n}_{m\sigma} = \hat{c}_{m\sigma}^\dagger \hat{c}_{m\sigma}$, U is the screened Coulomb interaction parameter, and J is the Hund's exchange coupling. The first three terms in Hamiltonian (1) correspond to the density-density part of Coulomb interaction and contain the exchange interaction in the Ising-type form. The remaining part consists of spin-flip (4th) and pair hopping (5th) terms. Using the z -projection of the spin operator, $\hat{S}_m^z = (\hat{n}_{m\uparrow} - \hat{n}_{m\downarrow})/2$, and the orbital occupancy operator, $\hat{N}_m = \hat{n}_{m\uparrow} + \hat{n}_{m\downarrow}$, the density-density part can be rewritten as

$$\begin{aligned} \hat{H}_{\text{dd}} = & U \sum_m \hat{n}_{m\uparrow} \hat{n}_{m\downarrow} \\ & + \frac{1}{2} \sum_{\substack{mm' \\ m \neq m'}} \{ \bar{U} \hat{N}_m \hat{N}_{m'} - 2J \hat{S}_m^z \hat{S}_{m'}^z \}, \end{aligned} \quad (2)$$

where $\bar{U} = U - 5J/2$ is the average value of the Coulomb interaction. The spin-flip term in Eq. (1) can be expressed via operators $\hat{S}_m^x = (\hat{c}_{m\uparrow}^\dagger \hat{c}_{m\downarrow} + \hat{c}_{m\downarrow}^\dagger \hat{c}_{m\uparrow})/2$ and $\hat{S}_m^y = -i(\hat{c}_{m\uparrow}^\dagger \hat{c}_{m\downarrow} - \hat{c}_{m\downarrow}^\dagger \hat{c}_{m\uparrow})/2$ as

$$\sum_\sigma \hat{c}_{m\sigma}^\dagger \hat{c}_{m\bar{\sigma}} \hat{c}_{m'\bar{\sigma}}^\dagger \hat{c}_{m'\sigma} = 2(\hat{S}_m^x \hat{S}_{m'}^x + \hat{S}_m^y \hat{S}_{m'}^y). \quad (3)$$

The pair hopping term acts only on high energy states with two electrons on the same orbital and thereby can be neglected. However, taking into account the spin-flip term in Eq. (1) is crucial for the correct description of spin dynamics. Therefore, the Coulomb interaction

Hamiltonian can be written as

$$\hat{H} = U \sum_m \hat{n}_{m\uparrow} \hat{n}_{m\downarrow} + \frac{1}{2} \sum_{\substack{mm' \\ m \neq m'}} \{\bar{U} \hat{N}_m \hat{N}_{m'} - 2J \hat{S}_m \hat{S}_{m'}\}. \quad (4)$$

Hamiltonian (4) with exchange term taken as a vector product, $J \hat{S}_m \hat{S}_{m'}$, is invariant with respect to the spin quantization axis rotations while the density-density counterpart with the Ising-type exchange term, $J \hat{S}_m^z \hat{S}_{m'}^z$, is not.

To restore the spin rotational symmetry of Hamiltonian (2) we here employ the method originally proposed by Hubbard.²³ The Coulomb interaction in Ref. 23 was considered in the following form:

$$U \hat{N}_\uparrow \hat{N}_\downarrow = \frac{1}{4} U \hat{N}^2 - U \hat{S}_z^2 = \frac{1}{4} U \hat{N}^2 - U (\vec{e} \hat{S})^2, \quad (5)$$

where $\hat{N}_\sigma = \sum_m \hat{n}_{m\sigma}$, $\hat{N} = \hat{N}_\uparrow + \hat{N}_\downarrow$, $\hat{S}_z = \sum_m \hat{S}_m^z$, \vec{S} is the total spin of the atom, and \vec{e} is an arbitrary unit vector that can be interpreted as a quantization axis direction. In order to restore the spin rotational symmetry in Eq. (5), averaging over all possible directions of \vec{e} was introduced using the functional integral technique.²³ Here we implement this method with the Hirsch-Fye quantum Monte Carlo algorithm (HF-QMC).²¹

The HF-QMC is based on the discrete Hubbard-Stratonovich transformation which employs the identity

$$\exp[-\Delta\tau U_{\mu\nu} \{\hat{n}_\mu \hat{n}_\nu - \frac{1}{2}(\hat{n}_\mu + \hat{n}_\nu)\}] = \frac{1}{2} \sum_{s_{\mu\nu}=\pm 1} \exp\{\lambda_{\mu\nu} s_{\mu\nu} (\hat{n}_\mu - \hat{n}_\nu)\}, \quad (6)$$

where μ and ν are combined spin-orbital indices, $s_{\mu\nu}$ is an Ising-like variable taking the values ± 1 , $U_{\mu\nu}$ stands for the matrix element of the Coulomb interaction operator, and $\lambda_{\mu\nu} = \text{arcosh}[\exp(\Delta\tau U_{\mu\nu}/2)]$. The imaginary time interval $[0, \beta]$ is divided into L slices of length $\Delta\tau$, so that $\tau_l = l\Delta\tau$, where $l = 1, 2, \dots, L$, and β denotes the inverse temperature.

Using the Trotter decomposition, the partition function of the system can be approximated as

$$Z = \text{Tr} e^{-\beta(\hat{H}_0 + \hat{H}_{\text{int}})} = \text{Tr} \prod_{l=1}^L e^{-\Delta\tau(\hat{H}_0 + \hat{H}_{\text{int}})} \simeq Z^{\Delta\tau} \equiv \text{Tr} \prod_{l=1}^L e^{-\Delta\tau \hat{H}_0} e^{-\Delta\tau \hat{H}_{\text{int}}}, \quad (7)$$

where \hat{H}_0 is the non-interacting (quadratic in fermion operators) part of Hamiltonian (1) and \hat{H}_{int} describes the Coulomb interaction. Therefore, the partition function can be written as a sum over all auxiliary field configurations:

$$Z^{\Delta\tau} = \frac{1}{2^{N_f L}} \sum_{\{s\}=\pm 1} z(s), \quad (8)$$

where $z(s)$ is the partition function for a particular configuration of auxiliary fields, $\{s\}$ denotes the set of all auxiliary fields, and $N_f = M(2M - 1)$ is the number of auxiliary fields for M orbitals.

In the case of the density-density form of the local Coulomb interaction, the single-electron dynamical potential has only the z component and can be expressed as

$$V_\mu(\tau_l) = \sum_{\nu(\neq\mu)} \lambda_{\mu\nu} s_{\mu\nu}(\tau_l) \sigma_{\mu\nu}, \quad (9)$$

$$\sigma_{\mu\nu} = \begin{cases} 1, & \mu < \nu \\ -1, & \mu > \nu \end{cases}. \quad (10)$$

For the quantization axis defined by polar angle θ and azimuthal angle ϕ , the single-electron dynamical potential can be written as

$$V'(\tau) = T^\dagger(\theta, \phi) V(\tau) T(\theta, \phi), \quad (11)$$

where $V(\tau)$ is the potential calculated by Eq. (9) for the quantization axis chosen to coincide with the z axis, and $T(\theta, \phi)$ stands for a transformation matrix in the spin variables and reads as

$$T(\theta, \phi) = \begin{pmatrix} \cos(\theta/2)e^{i\phi/2} & \sin(\theta/2)e^{-i\phi/2} \\ -\sin(\theta/2)e^{i\phi/2} & \cos(\theta/2)e^{-i\phi/2} \end{pmatrix}. \quad (12)$$

By integrating over all possible directions of the quantization axis, we obtain the partition function of the system with preserved spin rotational symmetry:

$$\tilde{Z}^{\Delta\tau} = \frac{1}{2^{1+N_f L} \pi^2} \sum_{\{s\}=\pm 1} \int_0^{2\pi} d\phi \int_0^\pi d\theta z(s, \theta, \phi). \quad (13)$$

Here, $z(s, \theta, \phi)$ is the partition function for a particular configuration of auxiliary fields with the quantization axis defined by angles θ and ϕ . Similarly to the original HF-QMC algorithm, it can be demonstrated that

$$z(s, \theta, \phi) = \det[G^{-1}(s, \theta, \phi)], \quad (14)$$

where $G(s, \theta, \phi)$ is the Green's function for a particular configuration of auxiliary fields, angles θ and ϕ . The resulting Green's function has the following form

$$\tilde{G}^{\Delta\tau} = \frac{C}{\tilde{Z}^{\Delta\tau}} \sum_{\{s\}=\pm 1} \int_0^{2\pi} d\phi \int_0^\pi d\theta G(s, \theta, \phi) z(s, \theta, \phi), \quad (15)$$

where $C = 1/(2^{1+N_f L} \pi^2)$. To integrate over all auxiliary field configurations and all possible directions of the quantization axis in Eq. (15), we employ the quantum Monte Carlo technique in which $\det[G^{-1}(s, \theta, \phi)]$ is interpreted as a stochastic weight. Similarly to the original HF-QMC algorithm, the Green's functions of two configurations with potentials V and V' are related to each other as

$$G' = A^{-1}G, \quad A = I + (I - G)(\exp(V' - V) - I), \quad (16)$$

where I denotes the unit matrix. However, in contrast to the HF-QMC, Eq. (16) now contains off-diagonal in the

spin indices elements. In the case of a single auxiliary spin-flip, the fast matrix update algorithm has the same form as in the HF-QMC method. Note, however, that all equations have the matrix form in the spin indices. The ratio of stochastic weights for two configurations which differ by the quantization axis direction can be calculated as

$$\frac{\det[G(s, \theta, \phi)]}{\det[G'(s, \theta', \phi')]} = \det[A]. \quad (17)$$

If the new quantization axis direction defined by angles θ' and ϕ' is accepted, the corresponding Green's function $G'(s, \theta', \phi')$ is calculated via the full update procedure using Eq. (16).

The physical meaning of the proposed rotationally invariant algorithm can be expressed as averaging over all possible directions of fluctuating spin polarization in the $3d$ shell, in contrast to polarization along the z -axis only in the density-density Hamiltonian. Thereby this technique allows one to take into account not only the longitudinal spin fluctuations but also the transverse ones.

III. RESULTS AND DISCUSSION

In this section, we first present results of our model calculations in comparison with previous studies. In particular, we employ the proposed approach to compute the two- and three-band Hubbard models on the infinite-dimensional Bethe lattice. We benchmark these calculations with the previously published results of the CT-QMC computations.¹⁰ To study the role of symmetry of the exchange interaction we compare our results with those obtained by employing the density-density form of the local Coulomb interaction. In particular, we compute the uniform magnetic susceptibility $\chi(T) = dM(T)/dH_z$ by calculating magnetization $M(T) = \sum_m (n_{m\uparrow} - n_{m\downarrow})$ induced by the external magnetic field H_z applied along the z axis (these calculations include the polarization of the impurity Weiss field). In our calculations, we adopted a few magnetic fields in the range from 0.01 to 0.04 eV to ensure linearity of response. The temperature dependence of magnetic susceptibility $\chi(T)$ is fitted to the Curie-Weiss law $\chi(T) = C/(T - T_C)$, where C is a material-specific constant and T_C is the Curie temperature. Next we investigate the electronic and magnetic properties of paramagnetic iron and nickel. We outline the importance of the correct spin rotational symmetry of the exchange interaction to describe the properties of these materials. These results are presented in Secs. III B and III C.

A. Two- and three-band models

In recent years the properties of the two- and three-orbital Hubbard models have been extensively investigated by using dynamical mean-field approach.^{9-11,24}

Here we would like to refer to Ref. 10 where the two- and three-orbital Hubbard models on the infinite-dimensional Bethe lattice were studied by means of the continuous-time quantum Monte Carlo method with full rotationally invariant Coulomb interaction. In particular, it was established that the effect of spin-flip interactions considerably depends on a band filling. It was shown that the Mott-Hubbard physics dominates due to the strong effective Coulomb interaction U in the particle-hole symmetric case, while away from half-filling formation of local magnetic moments is more plausible due to the Hund's exchange. In agreement with previous studies,¹¹⁻¹³ it was also shown that using the density-density form of the Coulomb interaction results in an overestimation of the magnetic transition temperature. For the benchmark purposes we here reproduce these calculations by employing the proposed rotationally invariant HF-QMC method.

In Fig. 1 (upper panel) we present our results for the inverse uniform magnetic susceptibility calculated for the two-band Hubbard model on the infinite-dimensional Bethe lattice. We have chosen the same set of parameters as in Ref. 10. Namely, we consider the two-band model at half-filling with $U = 4t$ for Coulomb interaction and $J = 1.2t$ for Hund's exchange, where t is a half of the non-interacting bandwidth. The calculated Curie temperatures are $0.49t$ and $0.39t$ for the conventional and rotationally invariant HF-QMC, respectively. These findings are in good quantitative agreement with the results of the CT-QMC calculations which give $T_C \sim 0.49t$ and $0.42t$ for the density-density and rotationally invariant interactions. Similar calculations with $U = 8t$ (see Table I) give $T_C \sim 0.49t$ and $0.36t$ for the density-density and rotationally invariant HF-QMC methods, respectively. We notice that the effective local moments calculated by the conventional and rotationally invariant HF-QMC methods agree well with those obtained by the CT-QMC.

To proceed further, we investigate the properties of the three-band Hubbard model with $U = 8t$ and $J = 1.2t$ at one-third electron filling (two-electron occupancy). In Fig. 1 (lower panel) we present our results for the inverse uniform magnetic susceptibility. Our results for $U = 4t$ and half-filling are summarized in Table I. For both sets of parameters, the broken rotational symmetry of the Coulomb interaction leads to an overestimation of the Curie temperature. However, in agreement with Ref. 10, this overestimation is found to be more pronounced at the $1/3$ filling than at the half-filling. This is due to the Hund's exchange interaction which plays a dominating role away from half-filling. The Curie temperatures calculated by the rotationally invariant HF-QMC algorithm are $0.69t$ and $0.15t$ for the $1/2$ and $1/3$ electron filling, respectively. These findings are in good quantitative agreement with the results of rotationally invariant CT-QMC calculations which give $0.70t$ and $0.14t$ for the half-filling and one-third filling, respectively. Our findings clearly indicate that the Curie temperature is overestimated by employing the density-density form of Coulomb interac-

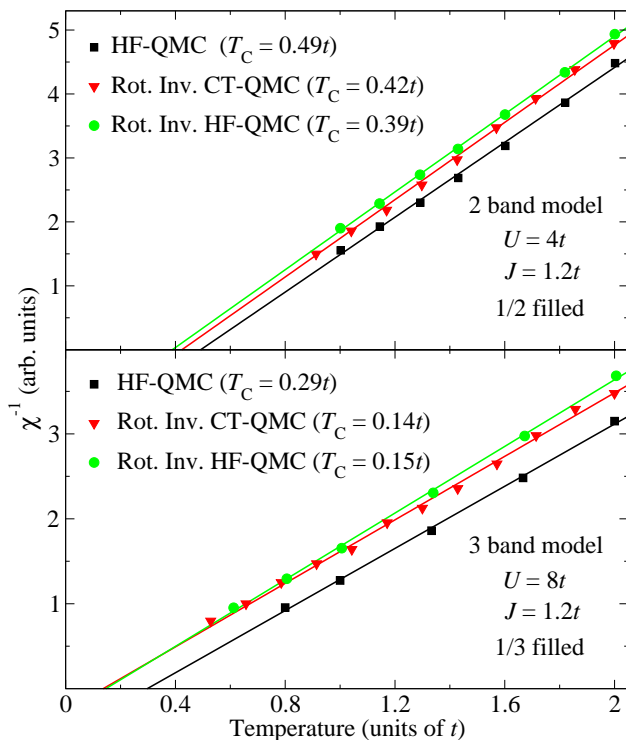


FIG. 1. (Color online) Temperature dependence of the inverse uniform magnetic susceptibility as obtained by DMFT for the two-band (upper panel) and three-band (lower panel) Hubbard models on the infinite-dimensional Bethe lattice. The straight lines depict the least-squares fit to the Curie-Weiss law. The extracted Curie temperatures and effective local magnetic moments are presented in Table I. The CT-QMC results were taken from Ref. 10.

tion. Hence, the retaining of spin rotational symmetry is crucial for the correct description of the magnetic transition temperature.

We find good quantitative agreement between the results obtained by rotationally invariant HF-QMC and CT-QMC methods. This demonstrates the validity of our method for accurate description of the magnetic properties of correlated electron systems. We note that transverse spin fluctuations can be regarded as an important source of magnetic response softening. It is expected that the proper treatment of the spin rotational symmetry of Coulomb interaction is even more important in the five-band case.

B. α iron

Elemental iron is one of the oldest and experimentally best studied itinerant ferromagnets. Various properties of iron can be understood on the basis of band-structure calculations.^{25,26} In particular, these calculations provide a good description of the low-temperature ferromagnetic phase of Fe. However, applications of conventional band-structure techniques to describe the properties of param-

TABLE I. Curie temperatures (in units of t) and effective local magnetic moments (in μ_B) as obtained by DMFT for the two- and three-band Hubbard models on the infinite-dimensional Bethe lattice. The results corresponding to the density-density interaction are denoted as HF-QMC and CT-QMC. The calculations were carried out with $J = 1.2t$. The CT-QMC results were taken from Ref. 10.

Bands	Filling	U/t	Impurity solver	T_C	μ_{eff}
2	1/2	4	CT-QMC	0.49	2.02
			HF-QMC	0.49	2.02
			Rot. Inv. CT-QMC	0.42	1.99
			Rot. Inv. HF-QMC	0.39	1.98
2	1/2	8	CT-QMC	0.50	2.21
			HF-QMC	0.49	2.22
			Rot. Inv. CT-QMC	0.40	2.20
			Rot. Inv. HF-QMC	0.36	2.19
3	1/2	4	CT-QMC	0.83	2.41
			HF-QMC	0.84	2.42
			Rot. Inv. CT-QMC	0.70	2.41
			Rot. Inv. HF-QMC	0.69	2.35
3	1/3	8	CT-QMC	0.27	2.54
			HF-QMC	0.29	2.56
			Rot. Inv. CT-QMC	0.14	2.55
			Rot. Inv. HF-QMC	0.15	2.48

agnetic iron, in particular, close to the $\alpha - \gamma$ phase transition, do not lead to satisfactory results. This is mainly due to the presence of local magnetic moments above the Curie temperature which are important for quantitative description of paramagnetic state. In this respect, the LDA+DMFT approach provides the best formalism which allows one to unify the localized and itinerant electron behavior in metallic magnets.

Applications of LDA+DMFT have shown to provide a good quantitative description of the electronic, magnetic, and structural properties of iron.^{7,8,27-32} However, an agreement was achieved only in terms of the reduced temperature T/T_C , while the calculated Curie temperature T_C was found to be almost twice larger than the experimental value of 1043 K (Ref. 33). Recently the properties of iron have been investigated by means of \vec{J} -QMC method, which uses the static approximation for the charge degrees of freedom and treats the exchange Coulomb interaction in the rotationally invariant form.¹³ These calculations indicate that substantial part of the Curie temperature overestimation comes from the approximate (density-density) treatment of the exchange Coulomb interaction.

We now calculate the electronic structure and magnetic properties of paramagnetic bcc iron by employing the LDA+DMFT implemented with the rotationally invariant HF-QMC method. We first calculate the non-magnetic LDA electronic structure of α iron using the tight-binding linear muffin-tin orbital (TB-LMTO) ap-

proach.³⁴ For these calculations we adopt lattice constant $a = 2.866 \text{ \AA}$. We construct an effective low-energy Hamiltonian in the basis of Fe *spd* Wannier orbitals using the N th-order muffin-tin (NMTO) method.³⁵ Here we adopt common definitions for the screened Coulomb interaction and Hund's exchange parameters in the $3d$ shell, namely, $U \equiv F^0$ and $J \equiv (F^2 + F^4)/14$, where F^0 , F^2 , and F^4 are the Slater integrals. We take $U = 2.3 \text{ eV}$ and $J = 0.9 \text{ eV}$ in accordance with the previous estimations^{7,27,28,36} and solve the five-orbital impurity problem within DMFT.

In Fig. 2 we present the partial density of states and the corresponding imaginary parts of the self-energies obtained by the rotationally invariant HF-QMC method at $T = 1160 \text{ K}$ in comparison with the non-magnetic LDA results. Our calculations reproduce the splitting in the density of states of the e_g orbitals near the Fermi level, which is absent in the LDA calculations. This result agrees well with the previous calculations^{13,27,28} as well as with the experimental data and is one of the characteristic features of α iron. The calculated self-energy for the t_{2g} states exhibits a Fermi-liquid-like behavior, whereas the e_g self-energy diverges at low frequencies. Our calculations with $J = 0$ recover the Fermi-liquid-like behavior for the e_g states resulting in the suppression of the splitting. This indicates that the splitting can be attributed to the exchange Coulomb interaction.²⁷ We found no evidence for the Hubbard subbands formation in the calculated quasiparticle spectrum. Thereby we conclude that in α iron the correlation effects are mainly affected by the strength of the Hund's coupling J rather than by the Coulomb interaction U which allow us to refer α iron as a Hund's metal. We note that importance of the Hund's exchange in multiorbital systems has been recently studied in Ref. 37.

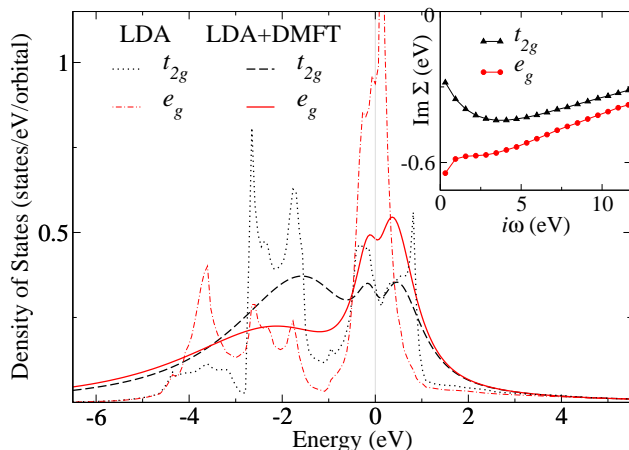


FIG. 2. (Color online) Partial t_{2g} (black) and e_g (red) densities of states for paramagnetic α iron as obtained by the rotationally invariant HF-QMC within LDA+DMFT in comparison with the non-magnetic LDA results. The Fermi level is indicated by the vertical (gray) line at zero energy. Inset: imaginary parts of the obtained self-energies.

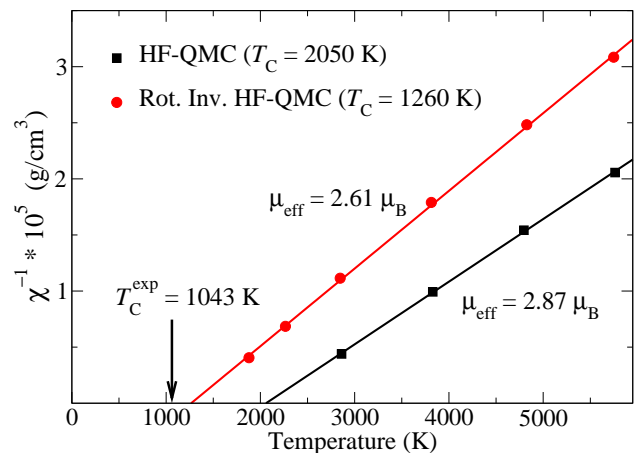


FIG. 3. (Color online) Temperature dependence of the inverse uniform magnetic susceptibility for α iron as obtained by the LDA+DMFT. The straight lines depict the least-squares fit to the Curie-Weiss law. The experimental value $T_C^{\text{exp}} = 1043 \text{ K}$ is denoted by the (black) arrow. The experimental value of the effective local magnetic moment is $\mu_{\text{eff}}^{\text{exp}} = 3.13 \mu_B$ (Ref. 33).

The temperature dependence of the inverse uniform magnetic susceptibility calculated by the LDA+DMFT shows a linear behavior at high temperatures (Fig. 3) in accordance with the Curie-Weiss law. It is clearly seen that the HF-QMC limited to the Ising-type exchange interaction substantially overestimates the Curie temperature value and yields $T_C \sim 2050 \text{ K}$. The rotationally invariant HF-QMC method gives $T_C \sim 1260 \text{ K}$, which is in good agreement with the experimental value of 1043 K (Ref. 33). The calculated values of the effective local moment extracted from the uniform magnetic susceptibility are $\mu_{\text{eff}} \sim 2.87 \mu_B$ and $2.61 \mu_B$ for the HF-QMC with density-density and rotationally invariant interactions, respectively. Our estimates are in reasonable agreement with the experimental value of $3.13 \mu_B$ (Ref. 33), which appears to be underestimated by both methods.

We note that preserving the spin rotational symmetry turns out to be crucial for quantitative description of magnetic properties of correlated materials. In particular, for α iron this leads to substantial improvement of the magnetic transition temperature value.

C. Nickel

Elemental nickel is another example of itinerant electron ferromagnets which together with iron serves as a benchmark material for electronic structure methods. Various low temperature properties of nickel can be understood by employing standard band-structure approaches.^{26,38} Nevertheless, these techniques generally fail to reproduce many characteristic features of nickel, such as an existence of satellite structure³⁹ at -6 eV , $3d$ electron bandwidth,⁴⁰ and the value of exchange splitting.⁴⁰ Applications of LDA+DMFT to study the elec-

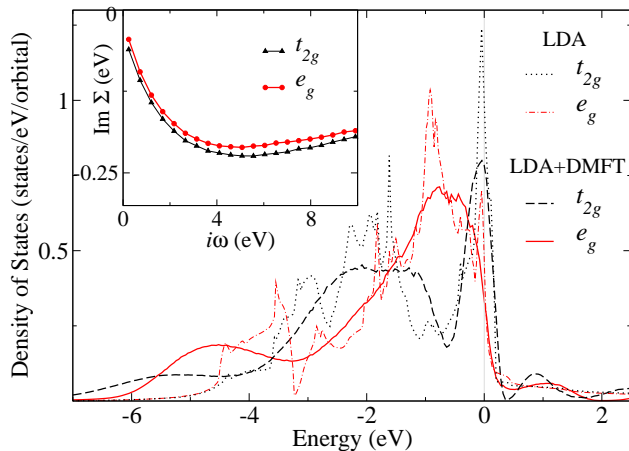


FIG. 4. (Color online) Partial densities of states for paramagnetic Ni obtained by rotationally invariant HF-QMC within LDA+DMFT in comparison with the LDA ones. The Fermi level is indicated by the vertical (gray) line at zero energy. Inset: imaginary parts of the obtained self-energies

tronic and magnetic properties of nickel have given a good quantitative description of many of these phenomena.^{7,28,30–32,41,42} The calculated magnetic properties of nickel are shown to be in good agreement with experiment. In contrast to iron, the overestimation of the magnetic transition temperature for nickel by LDA+DMFT with the Ising-type exchange interaction is not so significant.^{7,43} However, as demonstrated below, preserving the spin rotational symmetry leads to the underestimation of the Curie temperature.

We now compute the electronic structure and magnetic properties of paramagnetic nickel by employing the LDA+DMFT implemented with rotationally invariant HF-QMC method. To obtain the non-magnetic LDA electronic structure of fcc nickel we employ the tight-binding linear muffin-tin orbital approach. The calculations were performed for the lattice constant $a = 3.524 \text{ \AA}$. Using these results we construct an effective low-energy Hamiltonian in the basis of Ni *spd* Wannier orbitals by employing the NMTO method. In accordance with the previous estimations,^{31,42} we take $U = 2.3 \text{ eV}$ and $J = 1.0 \text{ eV}$ for the screened Coulomb interaction and Hund's exchange, respectively.

In Fig. 4 we present the partial densities of states and the imaginary parts of the self-energies obtained by the rotationally invariant algorithm at $T = 1160 \text{ K}$ in comparison with the non-magnetic LDA results. The inclusion of electronic correlations results in a small reduction of the bandwidth of nickel with respect to the non-magnetic LDA result. In addition, a satellite-like structure emerges at about -5.5 eV . In contrast to iron, the obtained self-energies for both the t_{2g} and e_g orbitals exhibit the Fermi-liquid-like behavior. This can also be seen from the calculated amplitudes of the effective damping $\Im\Sigma(0)$ which are -0.03 eV and -0.02 eV for the t_{2g} and e_g states of nickel, respectively, while $\Im\Sigma(0) \sim -0.24 \text{ eV}$

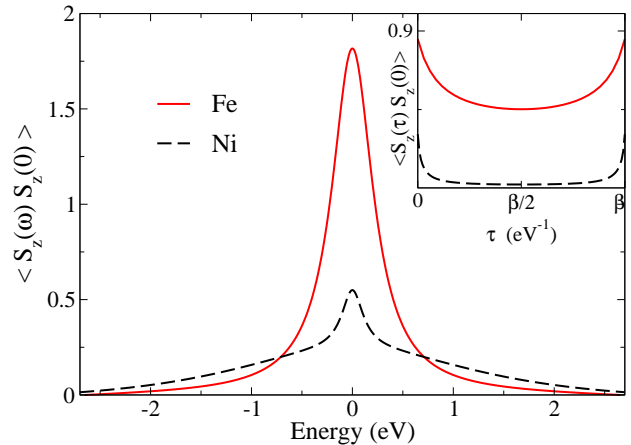


FIG. 5. (Color online) Spin-spin correlation functions on the real and imaginary (inset) energy axes for α iron and nickel calculated by LDA+DMFT at $T = 2.5 T_C$.

for the t_{2g} states of α iron. This indicates a more coherent nature of the electronic properties of nickel in comparison with iron. To quantify this qualitative difference^{7,43} we calculate spin-spin correlation functions for iron and nickel. In Fig. 5 we present the impurity spin-spin correlation functions on the real and imaginary energy axes calculated for α iron and nickel at $T = 2.5 T_C$ (T_C refers here to the corresponding calculated value of the Curie temperature). The height of peak on the real energy axis can be interpreted as a value of the local magnetic moment. The pronounced peak for iron indicates the presence of well localized magnetic moments above T_C , while magnetism of nickel is more itinerant.

In Fig. 6 we show the temperature dependence of the inverse uniform magnetic susceptibility calculated by LDA+DMFT. From these data we estimate the values of the Curie temperature. By employing the density-density approximation we find $T_C \sim 840 \text{ K}$, whereas the inclusion of the spin rotational symmetry leads to an almost twice smaller value of about 400 K . Both results are in reasonable agreement with the experimental value of 631 K . To proceed further, we compute the effective local magnetic moments by the HF-QMC and rotationally invariant methods which give $\mu_{\text{eff}} \sim 1.55 \mu_B$ and $1.49 \mu_B$, respectively. These findings are in good agreement with the experimental value of $1.62 \mu_B$ (Ref. 33). The fact that in α iron the LDA+DMFT with proper spin rotational symmetry results in an overestimated value of T_C , while it appears to be underestimated in nickel, can be dealt with non-local effects which are neglected in DMFT or with the more itinerant nature of magnetism in nickel than in α iron.

IV. CONCLUSIONS

In conclusion, we have presented an implementation of the LDA+DMFT approach which allows one to take

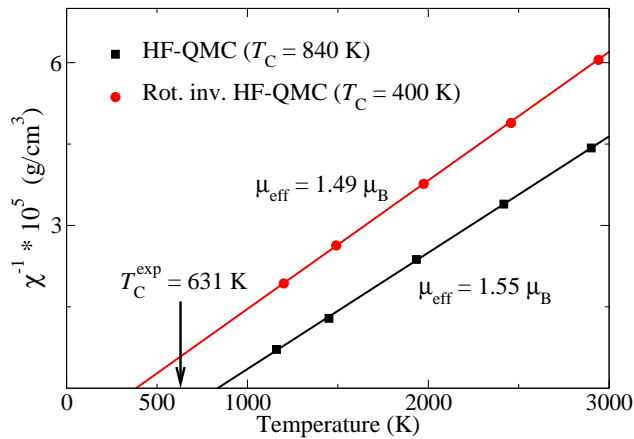


FIG. 6. (Color online) Temperature dependence of the inverse uniform magnetic susceptibility for Ni as obtained by LDA+DMFT. The straight lines depict the least-squares fit to the Curie-Weiss law. The experimental value $T_C^{\text{exp}} = 631$ K is denoted by the (black) arrow. The experimental value of the effective local magnetic moment is $\mu_{\text{eff}}^{\text{exp}} = 1.62 \mu_B$ (Ref. 33).

into account the spin rotational symmetry of the exchange Coulomb interaction. The computational scheme is based on extension of the Hirsch-Fye quantum Monte Carlo algorithm in which the spin rotational invariance of Hund's exchange is approximated by averaging over all possible directions of the spin quantization axis. The proposed approach provides a robust and computationally efficient method which allows us to compute high

temperature electronic properties of the five-orbital systems. We have used this approach to perform benchmark calculations for the two- and three-band Hubbard models on the infinite-dimensional Bethe lattice. Our results agree quantitatively well with those obtained using the continuous-time quantum Monte Carlo technique. The proposed method is employed to compute the electronic and magnetic properties of paramagnetic α iron and nickel. The obtained Curie temperatures agree well with experiment. Our results indicate that the density-density approximation for the Coulomb interaction leads to a substantial overestimation of the magnetic transition temperature.

ACKNOWLEDGMENTS

The authors thank T. Costi, E. Dagotto, A. Liebsch, A. Poteryaev, and S. Sakai for valuable comments. The authors are also grateful to A. Antipov for providing the CT-QMC data. This work was supported by the Russian Foundation for Basic Research (Projects Nos. 10-02-00046a, 12-02-91371-CT_a, 12-02-31207), the Ministry of education and science of Russian Federation through projects 14.A18.21.0076, 12.740.11.0026, the fund of the President of the Russian Federation for the support of scientific schools NSH-6172.2012.2, the Dynasty Foundation, Program of the Russian Academy of Science Presidium Quantum microphysics of condensed matter 12-P-2-1017, 12-M-23-2020. Support by the Deutsche Forschungsgemeinschaft through TRR 80 and FOR 1346 is gratefully acknowledged.

- ¹ W. Metzner and D. Vollhardt, Phys. Rev. Lett. **62**, 324 (1989); G. Kotliar and D. Vollhardt, Phys. Today **57**(3), 53 (2004); A. Georges, G. Kotliar, W. Krauth, and M. J. Rozenberg, Rev. Mod. Phys. **68**, 13 (1996).
- ² K. Held, I. A. Nekrasov, G. Keller, V. Eyert, N. Blümer, A. K. McMahan, R. T. Scalettar, Th. Pruschke, V. I. Anisimov, and D. Vollhardt, Phys. Status Solidi B **243**, 2599 (2006); K. Held, Adv. Phys. **56**, 829 (2007); J. Kunes, I. Leonov, M. Kollar, K. Byczuk, V. I. Anisimov, and D. Vollhardt, Eur. Phys. J. Special Topics **180**, 5 (2010); V. Anisimov and Y. Izyumov, *Electronic Structure of Strongly Correlated Materials* (Springer, Berlin, 2010).
- ³ M. Imada, A. Fujimori, and Y. Tokura, Rev. Mod. Phys. **70**, 1039 (1998).
- ⁴ V. I. Anisimov, A. I. Poteryaev, M. A. Korotin, A. O. Anokhin, and G. Kotliar, J. Phys. Condens. Matter **9**, 7359 (1997); A. I. Lichtenstein and M. I. Katsnelson, Phys. Rev. B **57**, 6884 (1998).
- ⁵ S. Biermann, A. Poteryaev, A. I. Lichtenstein, A. Georges, Phys. Rev. Lett. **94**, 026404 (2005); A. Kutepov, K. Haule, S. Y. Savrasov, and G. Kotliar, Phys. Rev. B **82**, 045105 (2010); B. Lazarovits, K. Kim, K. Haule, and G. Kotliar, *ibid.* **81**, 115117 (2010); A. S. Belozerov, M. A. Korotin, V. I. Anisimov, A. I. Poteryaev, *ibid.* **85**, 045109 (2012).
- ⁶ A. I. Lichtenstein and M. I. Katsnelson, Phys. Rev. B **62**, R9283 (2000); G. Kotliar, S. Y. Savrasov, G. Palsson, and G. Biroli, Phys. Rev. Lett. **87**, 186401 (2001); P. Sun and G. Kotliar, Phys. Rev. B **66**, 085120 (2002); S. Biermann, F. Aryasetiawan, and A. Georges, Phys. Rev. Lett. **90**, 086402 (2003); M. Potthoff, M. Aichhorn, and C. Dahnken, *ibid.* **91**, 206402 (2003); A. Toschi, A. A. Katantin, and K. Held, Phys. Rev. B **75**, 045118 (2007); A. N. Rubtsov, M. I. Katsnelson, and A. I. Lichtenstein, *ibid.* **77**, 033101 (2008).
- ⁷ A. I. Lichtenstein, M. I. Katsnelson, and G. Kotliar, Phys. Rev. Lett. **87**, 067205 (2001).
- ⁸ I. Leonov, A. I. Poteryaev, V. I. Anisimov, and D. Vollhardt, Phys. Rev. Lett. **106**, 106405 (2011); I. Leonov, A. I. Poteryaev, V. I. Anisimov, and D. Vollhardt, Phys. Rev. B **85**, 020401(R) (2012).
- ⁹ Th. Pruschke and R. Bulla, Eur. Phys. J. B **44**, 217 (2005).
- ¹⁰ A. E. Antipov, I. S. Krivenko, V. I. Anisimov, A. I. Lichtenstein, and A. N. Rubtsov, Phys. Rev. B **86**, 155107 (2012).
- ¹¹ S. Sakai, R. Arita, K. Held, and H. Aoki, Phys. Rev. B **74**, 155102 (2006).
- ¹² A. E. Antipov, M. S. Aleinikov, and V. I. Anisimov, JETP Lett. **94**, 126 (2011).

- ¹³ V. I. Anisimov, A. S. Belozerov, A. I. Poteryaev, I. Leonov, Phys. Rev. B **86**, 035152 (2012).
- ¹⁴ S. Sakai, R. Arita, and H. Aoki, Phys. Rev. Lett. **99**, 216402 (2007).
- ¹⁵ R. Bulla, T. A. Costi, and T. Pruschke, Rev. Mod. Phys. **80**, 395 (2008).
- ¹⁶ M. Caffarel and W. Krauth, Phys. Rev. Lett. **72**, 1545 (1994).
- ¹⁷ A. N. Rubtsov, V. V. Savkin, and A. I. Lichtenstein, Phys. Rev. B **72**, 035122 (2005); P. Werner, A. Comanac, L. de' Medici, M. Troyer, and A. J. Millis, Phys. Rev. Lett. **97**, 076405 (2006); K. Haule, Phys. Rev. B **75**, 155113 (2007); A. M. Lauchli and P. Werner, *ibid.* **80**, 235117 (2009); E. Gull *et al.*, Rev. Mod. Phys. **83**, 349 (2011).
- ¹⁸ S. Sakai, R. Arita, and H. Aoki, Phys. Rev. B **70**, 172504 (2004).
- ¹⁹ J. Kunes, D. M. Korotin, M. A. Korotin, V. I. Anisimov, and P. Werner, Phys. Rev. Lett. **102**, 146402 (2009); A. S. Belozerov, A. I. Poteryaev, and V. I. Anisimov, JETP Lett. **93**, 73 (2011).
- ²⁰ T. A. Costi *et al.*, Phys. Rev. Lett. **102**, 056802 (2009); E. Gorelov, T. O. Wehling, A. N. Rubtsov, M. I. Katsnelson, and A. I. Lichtenstein, Phys. Rev. B **80**, 155132 (2009); V. V. Mazurenko, S. N. Isakov, A. N. Rudenko, V. I. Anisimov, and A. I. Lichtenstein, *ibid.* **82**, 193403 (2010); M. Aichhorn, S. Biermann, T. Miyake, A. Georges, and M. Imada, *ibid.* **82**, 064504 (2010); Z. P. Yin, K. Haule, and G. Kotliar, Nature Mat. **10**, 932 (2011); B. Surer, M. Troyer, P. Werner, T. O. Wehling, A. M. Lauchli, A. Wilhelm, and A. I. Lichtenstein, Phys. Rev. B **85**, 085114 (2012).
- ²¹ J. E. Hirsch and R. M. Fye, Phys. Rev. Lett. **56**, 2521 (1986).
- ²² Strictly speaking, this parametrization of the Hamiltonian is appropriate for the two- and three-orbital systems. The five-band calculations require three effective Slater integrals (F^0 , F^2 , and F^4) which can be linked to the U and J parameters.
- ²³ J. Hubbard, Phys. Rev. B **19**, 2626 (1979); *ibid.* **20**, 4584 (1979).
- ²⁴ P. Werner and A. J. Millis, Phys. Rev. Lett. **99**, 126405 (2007); P. Werner, E. Gull, M. Troyer, and A. J. Millis, *ibid.* **101**, 166405 (2008); P. Werner, E. Gull, and A. J. Millis, Phys. Rev. B **79**, 115119 (2009).
- ²⁵ S. Y. Savrasov, Phys. Rev. Lett. **81**, 2570 (1998); D. J. Singh, W. E. Pickett, and H. Krakauer, Phys. Rev. B **43**, 11628 (1991); L. Stixrude, R. E. Cohen, and D. J. Singh, *ibid.* **50**, 6442 (1994).
- ²⁶ A. Dal Corso and S. de Gironcoli, Phys. Rev. B **62**, 273 (2000).
- ²⁷ A. A. Katanin, A. I. Poteryaev, A. V. Efremov, A. O. Shorikov, S. L. Skornyakov, M. A. Korotin, and V. I. Anisimov, Phys. Rev. B **81**, 045117 (2010).
- ²⁸ M. Katsnelson and A. Lichtenstein, J. Phys. Condens. Matter **11**, 1037 (1999).
- ²⁹ M. I. Katsnelson and A. I. Lichtenstein, Phys. Rev. B **61**, 8906 (2000).
- ³⁰ L. Chioncel, L. Vitos, I. A. Abrikosov, J. Kollar, M. I. Katsnelson, and A. I. Lichtenstein, Phys. Rev. B **67**, 235106 (2003).
- ³¹ D. Benea, J. Minar, L. Chioncel, S. Mankovsky, and H. Ebert, Phys. Rev. B **85**, 085109 (2012).
- ³² A. Grechnev, I. Di Marco, M. I. Katsnelson, A. I. Lichtenstein, J. Wills, and O. Eriksson, Phys. Rev. B **76**, 035107 (2007).
- ³³ *Ferromagnetic Materials*, edited by E. P. Wolfarth (North-Holland, Amsterdam, 1986), Vol. 1.
- ³⁴ O. K. Andersen and O. Jepsen, Phys. Rev. Lett. **53**, 2571 (1984); O. K. Andersen, Z. Pawlowska, and O. Jepsen, Phys. Rev. B **34**, 5253 (1986). The exchange-correlation potential was considered in the form of von Barth and Hedin [U. von Barth and L. Hedin, J. Phys. C **5**, 1629 (1972)] with the Langreth-Mehl-Hu non-local exchange correlation correction [C. D. Hu and D. C. Langreth, Phys. Scr. **32**, 391 (1985)].
- ³⁵ O. K. Andersen and T. Saha-Dasgupta, Phys. Rev. B **62**, 16219 (2000).
- ³⁶ M. Cococcioni and S. de Gironcoli, Phys. Rev. B **71**, 035105 (2005).
- ³⁷ L. de' Medici, J. Mravlje, and A. Georges, Phys. Rev. Lett. **107**, 256401 (2011).
- ³⁸ E. G. Moroni, G. Kresse, J. Hafner, and J. Furthmuller, Phys. Rev. B **56**, 15629 (1997); M. Cerny, J. Pokluda, M. Sob, M. Friak, and P. Sander, *ibid.* **67**, 035116 (2003).
- ³⁹ C. Guillot *et al.*, Phys. Rev. Lett. **39**, 1632 (1977).
- ⁴⁰ D. E. Eastman, F. J. Himpsel, and J. A. Knapp, Phys. Rev. Lett. **40**, 1514 (1978); F. J. Himpsel, J. A. Knapp, and D. E. Eastman, Phys. Rev. B **19**, 2919 (1979).
- ⁴¹ J. Minar, L. Chioncel, A. Perlov, H. Ebert, M. I. Katsnelson, and A. I. Lichtenstein, Phys. Rev. B **72**, 045125 (2005); J. Braun, J. Minar, H. Ebert, M. I. Katsnelson, and A. I. Lichtenstein, Phys. Rev. Lett. **97**, 227601 (2006); I. Di Marco, J. Minar, S. Chadov, M. I. Katsnelson, H. Ebert, and A. I. Lichtenstein, Phys. Rev. B **79**, 115111 (2009); J. Minar, J. Phys. Condens. Matter **23**, 253201 (2011); J. Kolorenc, A. I. Poteryaev, and A. I. Lichtenstein, Phys. Rev. B **85**, 235136 (2012).
- ⁴² M. I. Katsnelson and A. I. Lichtenstein, Eur. Phys. J. B **30**, 9 (2002).
- ⁴³ M. I. Katsnelson and A. I. Lichtenstein, J. Phys.: Condens. Matter **16**, 7439 (2004).